

# Quasiparticle States near the Surface and the Domain Wall in a $p_x \pm ip_y$ -Wave Superconductor

Masashige MATSUMOTO and Manfred SIGRIST<sup>1</sup>

*Department of Physics, Faculty of Science, Shizuoka University, 836 Oya, Shizuoka 422-8529, Japan*

<sup>1</sup>*Yukawa Institute for Theoretical Physics, Kyoto University, Kyoto 606-8502, Japan*

(Received )

The electronic states near a surface or a domain wall in the  $p$ -wave superconductor are studied for the order parameter of the form  $p_x \pm ip_y$ -wave, which is a unitary odd-parity state with broken time-reversal symmetry. This state has been recently suggested as the superconducting state of  $\text{Sr}_2\text{RuO}_4$ . The spatial variation of the order parameter and vector potential is determined self-consistently within the quasi-classical approximation. The local density of states at the surface is constant and does not show any peak-like or gap-like structure within the superconducting energy gap, in contrast to the case of the  $d$ -wave superconductors. The influence of an external magnetic field is mainly observable in the energy range above the bulk gap. On the other hand, there is a small energy gap in the local density of states at the domain wall between domains of the two degenerate  $p_x + ip_y$ -wave and  $p_x - ip_y$ -wave states.

KEYWORDS:  $\text{Sr}_2\text{RuO}_4$ ,  $p$ -wave superconductor, unitary state, time-reversal breaking state, boundary effect, surface, domain wall, quasi-classical theory, Ginzburg-Landau free energy

## §1. Introduction

$\text{Sr}_2\text{RuO}_4$  is the first superconductor with layered perovskite structure, which does not contain copper.<sup>1)</sup> Although the structure is identical to that of some of the high-temperature superconductors, the transition temperature is rather low,  $T_C=1.5\text{K}$ . There is a clear difference in the electronic structure, since  $\text{Sr}_2\text{RuO}_4$  is a good metal and even a Fermi liquid in its stoichiometric composition. Band structure calculations in good agreement with the de Haas-van Alphen measurements show that this compound has three Fermi surfaces originating from the three  $4d-t_{2g}$ -orbitals of  $\text{Ru}^{4+}$ .<sup>2,3,4)</sup> There is growing experimental evidence that the superconducting state is unconventional (non- $s$ -wave). Examples are the absence of a Hebel-Slichter peak in  $1/T_1T$  of NQR-measurements<sup>5)</sup> and the sensitivity of  $T_C$  on non-magnetic impurities.<sup>6)</sup>

It was suggested that the superconducting state has odd-parity (spin triplet) pairing.<sup>7,8,10,9,11)</sup> There is a certain similarity with  $^3\text{He}$  considering the correlation effects (superfluid  $^3\text{He}$  has  $p$ -wave pairing).<sup>7)</sup> Furthermore, there is a series of related compounds such as  $\text{SrRuO}_3$  which are

ferromagnetic suggesting that ferromagnetic spin fluctuations are probably enhanced in  $\text{Sr}_2\text{RuO}_4$  and mediate odd-parity, spin triplet pairing.<sup>12,7,13)</sup> The recent discovery of intrinsic magnetism in the superconducting phase by  $\mu\text{SR}$  experiments indicates a pairing state with broken time reversal symmetry.<sup>14)</sup> Symmetry considerations lead to the conclusion that this would only be possible for an odd-parity state.<sup>15)</sup> A very strong support for odd-parity pairing comes also from the Knight shift data in the  $^{17}\text{O}$ -NMR measurements which demonstrate the absence of any reduction of the spin susceptibility in the superconducting state.<sup>16)</sup> The superconducting state compatible with all of these experiments is given by  $\mathbf{d}(\mathbf{k})=\hat{\mathbf{z}}(k_x\pm ik_y)$ .<sup>15)</sup>

The presence of three electron bands forming the Fermi liquid state leads to the question whether all of them contribute to superconductivity on equal terms. Symmetry considerations show that it is possible to separate the orbitals  $\{4d_{yz}, 4d_{zx}\}$  (forming two Fermi surfaces) and  $4d_{xy}$  (forming one Fermi surface). Thus it is theoretically possible that superconductivity predominantly appears in one of the two sets of orbitals, while the other participates passively only through induced superconductivity.<sup>17)</sup> There are several supporting experiments for the scenario of “orbital dependent superconductivity”. The specific heat<sup>18)</sup> and NQR experiments<sup>5)</sup> indicate a considerable residual density of states in the superconducting state which could be attributed to the passive electron bands. Furthermore, the analysis of the London penetration depth extrapolated to the zero temperature is compatible with taking only one of the two subsets of orbitals into account for the superconducting state.<sup>19)</sup> The present experimental situation is compatible with a superconducting state dominantly in the  $4d_{xy}$ -orbital. The recent prediction of a square form of the vortex lattice aligned with the crystal lattice axis was confirmed experimentally and is consistently explained with the assumption of superconductivity in the  $4d_{xy}$ -orbital as well.<sup>20,19)</sup> It seems therefore to be justified to approximate the electronic structure by a single band model consisting a single practically cylinder-shaped Fermi surface.

The theoretical study of boundary effects in high-temperature superconductors with  $d$ -wave Cooper pairing have turned out to be very fruitful for subsequent experimental investigations. The bound states cause unusual features in the Andreev reflection and tunneling spectroscopy.<sup>21,22,23,24,25,26,27)</sup> Recently characteristic tunneling conductance properties were examined theoretically for the triplet pairing states.<sup>28,29)</sup> Conductance peak features related to the bound states are very sensitive to the angle of the incidence in this case, in contrast to the  $d$ -wave superconductor. In this paper we investigate the electronic states near the surface and compare them with those found near domain walls. Domain walls appear due to the fact that the superconducting state is two-fold degenerate ( $p_x+ip_y$ - and  $p_x-ip_y$ -wave state) such that two types of domains are possible. Because of the discrete degeneracy the separating domain walls are very well localized and constitute a region of spatial deformation of the order parameter giving rise to subgap quasiparticle states analogous to the surface.

## §2. The Quasiclassical Formulation

In this paper we study boundary effects in the  $p$ -wave superconductor, determining the order parameters self-consistently. For this purpose we use the quasi-classical Green function formalism developed by Schopohl, which, for example, has been applied to the vortex problem.<sup>30,31)</sup> We adapt this scheme to the boundary problem and apply it to both the case of the surface and the domain wall.

For simplicity we assume that the superconductor is two-dimensional with a single cylindrical Fermi surface which is a reasonable first approximation to the band of the  $4d_{xy}$ -orbital, and that the superconducting order parameter has a  $p$ -wave symmetry. The gap matrix for the  $p$ -wave state is given by the  $\mathbf{d}$ -vector defined as

$$\hat{\Delta}(\mathbf{r}, \mathbf{r}') = i\mathbf{d}(\mathbf{r}, \mathbf{r}') \cdot \hat{\sigma} \hat{\sigma}_y, \quad (2.1)$$

where  $\hat{\sigma}_i (i=x, y, z)$  is the Pauli spin matrix. We restrict ourselves to the case of  $\mathbf{d}(\mathbf{r}, \mathbf{r}') = (0, 0, \Delta(\mathbf{r}, \mathbf{r}'))$  type, so that the Bogoliubov-de Gennes equation reduces to a  $2 \times 2$  matrix form,

$$\int d\mathbf{r}' \begin{pmatrix} \delta(\mathbf{r} - \mathbf{r}')h_0(\mathbf{r}') & \Delta(\mathbf{r}, \mathbf{r}') \\ -\Delta^*(\mathbf{r}, \mathbf{r}') & -\delta(\mathbf{r} - \mathbf{r}')h_0^*(\mathbf{r}') \end{pmatrix} \begin{pmatrix} u_l(\mathbf{r}') \\ v_l(\mathbf{r}') \end{pmatrix} = E_l \begin{pmatrix} u_l(\mathbf{r}) \\ v_l(\mathbf{r}) \end{pmatrix}. \quad (2.2)$$

Here  $\Delta(\mathbf{r}, \mathbf{r}')$  is the  $p$ -wave pair potential,  $E_l$  is the  $l$ -th energy eigenvalue, and  $h_0(\mathbf{r}) = [-i\nabla + e\mathbf{A}(\mathbf{r})]^2/2m - E_F$  is the kinetic energy of an electron measured from the Fermi energy, with  $e$  ( $e > 0$ ) and  $\mathbf{A}$  as the charge of the electron and vector potential, respectively. For convenience  $\hbar$  is taken to be unity throughout this paper.

Introducing the Andreev approximation (i.e. separating the rapid oscillations) as

$$\begin{pmatrix} u_l(\mathbf{r}) \\ v_l(\mathbf{r}) \end{pmatrix} = \begin{pmatrix} \bar{u}_l(\mathbf{k}_F, \mathbf{r}) \\ \bar{v}_l(\mathbf{k}_F, \mathbf{r}) \end{pmatrix} e^{i\mathbf{k}_F \cdot \mathbf{r}}, \quad (2.3)$$

we obtain the Andreev equation,<sup>32,33)</sup>

$$\begin{pmatrix} -i\mathbf{v}_F \cdot \nabla + e\mathbf{v}_F \cdot \mathbf{A}(\mathbf{r}) & \Delta(\mathbf{k}_F, \mathbf{r}) \\ -\Delta^*(-\mathbf{k}_F, \mathbf{r}) & i\mathbf{v}_F \cdot \nabla + e\mathbf{v}_F \cdot \mathbf{A}(\mathbf{r}) \end{pmatrix} \begin{pmatrix} \bar{u}_l(\mathbf{k}_F, \mathbf{r}) \\ \bar{v}_l(\mathbf{k}_F, \mathbf{r}) \end{pmatrix} = E_l \begin{pmatrix} \bar{u}_l(\mathbf{k}_F, \mathbf{r}) \\ \bar{v}_l(\mathbf{k}_F, \mathbf{r}) \end{pmatrix}, \quad (2.4)$$

where  $\mathbf{k}_F$  and  $\mathbf{v}_F$  are the Fermi wave number and the Fermi velocity, respectively. The  $\mathbf{k}_F$  dependence of  $\Delta(\mathbf{k}_F, \mathbf{r})$  represents the symmetry of the order parameter and  $\mathbf{r}$  is the center position of the Cooper pair. Due to the  $p$ -wave symmetry (i.e.  $\Delta(-\mathbf{k}_F, \mathbf{r}) = -\Delta(\mathbf{k}_F, \mathbf{r})$ ), eq. (2.4) has the same form as the Andreev equation in the case of singlet pairing. The corresponding Eilenberger equation is given by

$$-i\mathbf{v}_F \cdot \nabla \hat{g}(\mathbf{k}_F, \omega_m, \mathbf{r}) = \left[ \begin{pmatrix} i\omega_m - e\mathbf{v}_F \cdot \mathbf{A}(\mathbf{r}) & -\Delta(\mathbf{k}_F, \mathbf{r}) \\ \Delta^*(\mathbf{k}_F, \mathbf{r}) & -i\omega_m + e\mathbf{v}_F \cdot \mathbf{A}(\mathbf{r}) \end{pmatrix}, \hat{g}(\mathbf{k}_F, \omega_m, \mathbf{r}) \right], \quad (2.5)$$

where  $\hat{g}(\mathbf{k}_F, \omega_m, \mathbf{r})$  is the quasi-classical Green function in a  $2 \times 2$  matrix form and  $\omega_m = \pi T(2m+1)$  ( $m$ : integer) is the fermion Matsubara frequency.<sup>34,35,36)</sup> For simplicity the Boltzmann constant is

taken to be unity. The equations for the matrix elements of the quasi-classical Green function are expressed as

$$\begin{aligned}
\hat{g}(\mathbf{k}_F, \omega_m, \mathbf{r}) &= \begin{pmatrix} g(\mathbf{k}_F, \omega_m, \mathbf{r}) & if(\mathbf{k}_F, \omega_m, \mathbf{r}) \\ -i\bar{f}(\mathbf{k}_F, \omega_m, \mathbf{r}) & -g(\mathbf{k}_F, \omega_m, \mathbf{r}) \end{pmatrix}, \\
\mathbf{v}_F \cdot \nabla g(\mathbf{k}_F, \omega_m, \mathbf{r}) &= \Delta^*(\mathbf{k}_F, \mathbf{r})f(\mathbf{k}_F, \omega_m, \mathbf{r}) - \Delta(\mathbf{k}_F, \mathbf{r})\bar{f}(\mathbf{k}_F, \omega_m, \mathbf{r}), \\
(\omega_m + ie\mathbf{v}_F \cdot \mathbf{A}(\mathbf{r}) + \frac{1}{2}\mathbf{v}_F \cdot \nabla)f(\mathbf{k}_F, \omega_m, \mathbf{r}) &= \Delta(\mathbf{k}_F, \mathbf{r})g(\mathbf{k}_F, \omega_m, \mathbf{r}), \\
(\omega_m + ie\mathbf{v}_F \cdot \mathbf{A}(\mathbf{r}) - \frac{1}{2}\mathbf{v}_F \cdot \nabla)\bar{f}(\mathbf{k}_F, \omega_m, \mathbf{r}) &= \Delta^*(\mathbf{k}_F, \mathbf{r})g(\mathbf{k}_F, \omega_m, \mathbf{r}).
\end{aligned} \tag{2.6}$$

These equations contain the following symmetries,

$$\begin{aligned}
g(-\mathbf{k}_F, \omega_m, \mathbf{r}) &= g^*(\mathbf{k}_F, \omega_m, \mathbf{r}), & g(\mathbf{k}_F, -\omega_m, \mathbf{r}) &= -g^*(\mathbf{k}_F, \omega_m, \mathbf{r}), \\
f(-\mathbf{k}_F, \omega_m, \mathbf{r}) &= -\bar{f}^*(\mathbf{k}_F, \omega_m, \mathbf{r}), & f(\mathbf{k}_F, -\omega_m, \mathbf{r}) &= \bar{f}^*(\mathbf{k}_F, \omega_m, \mathbf{r}).
\end{aligned} \tag{2.7}$$

Using the following transformation, we can solve the Eilenberger equation in a simple way,<sup>30)</sup>

$$\begin{aligned}
g(\mathbf{k}_F, \omega_m, \mathbf{r}) &= \frac{1 - a(\mathbf{k}_F, \omega_m, \mathbf{r})b(\mathbf{k}_F, \omega_m, \mathbf{r})}{1 + a(\mathbf{k}_F, \omega_m, \mathbf{r})b(\mathbf{k}_F, \omega_m, \mathbf{r})}, \\
f(\mathbf{k}_F, \omega_m, \mathbf{r}) &= \frac{2a(\mathbf{k}_F, \omega_m, \mathbf{r})}{1 + a(\mathbf{k}_F, \omega_m, \mathbf{r})b(\mathbf{k}_F, \omega_m, \mathbf{r})}, \\
\bar{f}(\mathbf{k}_F, \omega_m, \mathbf{r}) &= \frac{2b(\mathbf{k}_F, \omega_m, \mathbf{r})}{1 + a(\mathbf{k}_F, \omega_m, \mathbf{r})b(\mathbf{k}_F, \omega_m, \mathbf{r})},
\end{aligned} \tag{2.8}$$

where  $a$  and  $b$  satisfy

$$\begin{aligned}
\mathbf{v}_F \cdot \nabla a(\mathbf{k}_F, \omega_m, \mathbf{r}) &= \Delta(\mathbf{k}_F, \mathbf{r}) - \Delta^*(\mathbf{k}_F, \mathbf{r})a^2(\mathbf{k}_F, \omega_m, \mathbf{r}) - 2[\omega_m + ie\mathbf{v}_F \cdot \mathbf{A}(\mathbf{r})]a(\mathbf{k}_F, \omega_m, \mathbf{r}), \\
\mathbf{v}_F \cdot \nabla b(\mathbf{k}_F, \omega_m, \mathbf{r}) &= -\Delta^*(\mathbf{k}_F, \mathbf{r}) + \Delta(\mathbf{k}_F, \mathbf{r})b^2(\mathbf{k}_F, \omega_m, \mathbf{r}) + 2[\omega_m + ie\mathbf{v}_F \cdot \mathbf{A}(\mathbf{r})]b(\mathbf{k}_F, \omega_m, \mathbf{r}).
\end{aligned} \tag{2.9}$$

Let us now consider the case of a surface perpendicular to the  $x$ -direction. We assume that quasi-particles are specularly reflected at the surface. We solve eq. (2.9) along the classical trajectories as shown in Fig. 1(a) where the quasiparticle moves with the momentum close to  $\mathbf{k}_{F1}$  from A to B and with momentum  $\mathbf{k}_{F2}$  from B to C. Since the surface is specular and translational invariant along the  $y$ - and  $z$ -direction, the incident momentum along the surface is conserved. We then match the two solutions using the boundary condition of the quasi-classical Green function at point B given by<sup>35, 36)</sup>

$$\hat{g}(\mathbf{k}_{F1}, \omega_m, B) = \hat{g}(\mathbf{k}_{F2}, \omega_m, B), \tag{2.10}$$

which for  $a$  and  $b$  means,

$$a(\mathbf{k}_{F1}, \omega_m, B) = a(\mathbf{k}_{F2}, \omega_m, B), \quad b(\mathbf{k}_{F1}, \omega_m, B) = b(\mathbf{k}_{F2}, \omega_m, B). \tag{2.11}$$

Since the system is translationally invariant perpendicular to the  $x$ -axis, the quasi-classical Green function or  $a(\mathbf{k}_F, \omega_m, \mathbf{r})$  and  $b(\mathbf{k}_F, \omega_m, \mathbf{r})$  depend only on  $x$ . Thus eq. (2.9) can be rewritten as

$$\frac{d}{dx}a(\mathbf{k}_F, \omega_m, x) = \frac{1}{v_{Fx}} \left\{ \Delta(\mathbf{k}_F, x) - \Delta^*(\mathbf{k}_F, x)a^2(\mathbf{k}_F, \omega_m, x) - 2[\omega_m + ie\mathbf{v}_{Fy}A_y(x)]a(\mathbf{k}_F, \omega_m, x) \right\},$$

$$\frac{d}{dx}b(\mathbf{k}_F, \omega_m, x) = \frac{1}{v_{Fx}} \left\{ -\Delta^*(\mathbf{k}_F, x) + \Delta(\mathbf{k}_F, x)b^2(\mathbf{k}_F, \omega_m, x) + 2[\omega_m + ie v_{Fy} A_y(x)]b(\mathbf{k}_F, \omega_m, x) \right\}. \quad (2.12)$$

where  $v_{Fx}$  and  $v_{Fy}$  are the  $x$  and  $y$  component of the Fermi velocity, respectively. The initial and boundary conditions for eq. (2.12) are given by

$$\begin{aligned} a(\mathbf{k}_{F1}, \omega_m, x = \infty) &= \frac{\Delta(\mathbf{k}_{F1}, \infty)}{\sqrt{[\omega_m + ie v_{Fy} A_y(\infty)]^2 + |\Delta(\mathbf{k}_{F1}, \infty)|^2 + \omega_m + ie v_{Fy} A_y(\infty)}}, \\ b(\mathbf{k}_{F2}, \omega_m, x = \infty) &= \frac{\Delta^*(\mathbf{k}_{F2}, \infty)}{\sqrt{[\omega_m + ie v_{Fy} A_y(\infty)]^2 + |\Delta(\mathbf{k}_{F2}, \infty)|^2 + \omega_m + ie v_{Fy} A_y(\infty)}}, \\ a(\mathbf{k}_{F1}, \omega_m, x = 0) &= a(\mathbf{k}_{F2}, \omega_m, x = 0), \\ b(\mathbf{k}_{F1}, \omega_m, x = 0) &= b(\mathbf{k}_{F2}, \omega_m, x = 0). \end{aligned} \quad (2.13)$$

The position-dependent order parameter can be determined by the quasi-classical Green function. The gap equations for the  $p_x$ - and  $p_y$ -wave (i.e.  $\Delta(\mathbf{k}_F, x) = \Delta_x(x) \cos \theta_k + \Delta_y(x) \sin \theta_k$ ) are given (using eq. (2.7)) as<sup>33,37)</sup>

$$\begin{aligned} \begin{pmatrix} \Delta_x(x) \\ \Delta_y(x) \end{pmatrix} &= \pi T \sum_{|\omega_m| < \omega_C} \frac{1}{2\pi} \int_{-\pi}^{\pi} d\theta_k \begin{pmatrix} 2V_p \cos \theta_k \\ 2V_p \sin \theta_k \end{pmatrix} f(\theta_k, \omega_m, x) \\ &= \pi T V_p \sum_{0 < \omega_m < \omega_C} \frac{1}{\pi} \int_0^{\pi} d\theta_k \begin{pmatrix} 2 \cos \theta_k \\ 2 \sin \theta_k \end{pmatrix} [f(\theta_k, \omega_m, x) + \bar{f}^*(\theta_k, \omega_m, x)] \\ &= \pi T V_p \sum_{0 < \omega_m < \omega_C} \frac{1}{\pi} \int_0^{\frac{\pi}{2}} d\theta_k \\ &\quad \times \begin{pmatrix} 2 \cos \theta_k [f(\theta_k, \omega_m, x) + \bar{f}^*(\theta_k, \omega_m, x) - f(\pi - \theta_k, \omega_m, x) - \bar{f}^*(\pi - \theta_k, \omega_m, x)] \\ 2 \sin \theta_k [f(\theta_k, \omega_m, x) + \bar{f}^*(\theta_k, \omega_m, x) + f(\pi - \theta_k, \omega_m, -x) + \bar{f}^*(\pi - \theta_k, \omega_m, -x)] \end{pmatrix}, \\ V_p &= \frac{1}{\log \frac{T}{T_C} + \sum_{0 < m < \omega_C / 2\pi T} \frac{1}{m-1/2}}, \end{aligned} \quad (2.14)$$

where  $\theta_k$  is the angle of the Fermi momentum measured from the  $k_x$ -axis and  $\omega_C$  is the cutoff energy. We write  $\Delta_x$  and  $\Delta_y$  for the order parameter components corresponding to the  $p_x$ - and  $p_y$ -wave, respectively. Generally, they are complex numbers.  $T_C$  is the superconducting transition temperature which we assume is the same for both components.

The supercurrent due to the broken time-reversal symmetry is a general property, which was previously studied in the framework of Ginzburg-Landau (GL) theory.<sup>38,39)</sup> Here we investigate it within the quasi-classical approximation. The current density along the  $y$  direction can be expressed by the quasi-classical Green function,

$$\begin{aligned} J_y(x) &= -ev_F N(0) T \sum_{|\omega_m| < \omega_C} \frac{1}{2\pi} \int_{-\pi}^{\pi} d\theta_k \sin \theta_k (-i\pi) g(\theta_k, \omega_m, x) \\ &= -2ev_F N(0) T \sum_{0 < \omega_m < \omega_C} \int_0^{\frac{\pi}{2}} d\theta_k \sin \theta_k \text{Im} [g(\theta_k, \omega_m, x) + g(\pi - \theta_k, \omega_m, x)], \end{aligned} \quad (2.15)$$

where the symmetry relations of eq. (2.7) have been used.<sup>40,41)</sup>  $N(0)$  is the normal state density of states per unit volume at  $E_F$  and  $n$  is the density of electrons, whereby both  $N(0)$  and  $n$  include up and down spin electrons.

The magnetic field and vector potential are calculated using the Maxwell equation. The magnetic field and the vector potential can be determined as follows:

$$B_z(x) = -\mu \int_0^x dx' J_y(x'), \quad A_y(x) = \mu \int_0^x dx' B_z(x') - \mu \int_0^\infty dx' B_z(x'), \quad (2.16)$$

with  $\mu$  as the permeability. Equation (2.16) is chosen to satisfy the boundary conditions of  $B_z(0)=0$ ,  $A_y(\infty)=0$ . Now we can solve the gap equation (2.14) iteratively by using eqs. (2.8), (2.12), (2.13), (2.15) and (2.16) until the self-consistency is achieved.

### §3. Quasiparticle Properties at the Surface

#### 3.1 Self-consistent solution

Before examining the boundary effect, let us study first the bulk case, where  $f$  and  $\bar{f}$  in the bulk are given by

$$f(\theta_k, \omega_m, \text{bulk}) = \bar{f}^*(\theta_k, \omega_m, \text{bulk}) = \frac{\Delta(\theta_k, \text{bulk})}{\sqrt{\omega_m^2 + |\Delta(\theta_k, \text{bulk})|^2}},$$

$$\Delta(\theta_k, \text{bulk}) = \Delta_x(\text{bulk}) \cos \theta_k + i\Delta_y(\text{bulk}) \sin \theta_k. \quad (3.1)$$

Here we have assumed real values for  $\Delta_x$  and  $\Delta_y$ , since we are interested in the  $p_x+ip_y$ -wave state. Substituting eq. (3.1) into the gap equation, we can obtain the bulk solution at  $T=0$ :

$$\Delta_x(\text{bulk}) = \Delta_y(\text{bulk}) = \Delta(0) = 2\omega_C e^{-\frac{1}{v_p}}, \quad T_C = \frac{2e^\gamma \omega_C}{\pi} e^{-\frac{1}{v_p}}, \quad \frac{\Delta(0)}{T_C} = \pi e^{-\gamma} \simeq 1.76. \quad (3.2)$$

Here  $\gamma$  is the Euler's constant:  $\gamma=0.57721\dots$ . This solution is similar to the  $s$ -wave case, since  $|\Delta(\theta_k, \text{bulk})|$  is a constant on the Fermi surface. If one of the two order parameter components is absent, the solution becomes

$$\Delta_x(\text{bulk}) = 0, \quad \Delta_y(\text{bulk}) = \Delta_{\text{single}}(0) = 4\omega_C e^{-(\frac{1}{v_p} + \frac{1}{2})},$$

$$T_C = \frac{2e^\gamma \omega_C}{\pi} e^{-\frac{1}{v_p}}, \quad \frac{\Delta_{\text{single}}(0)}{T_C} = 2e^{-\frac{1}{2}} \pi e^{-\gamma} \simeq 2.14. \quad (3.3)$$

Note that  $\Delta_{\text{single}}(0)$  is larger than  $\Delta(0)$ . This is due to the fact that there are gapless points on the Fermi surface for the single existing solution and that the denominators of  $f$  and  $\bar{f}$  become small. Though  $\Delta(0)$  is small, its solution is more stable, since it opens a gap everywhere on the Fermi surface.<sup>13)</sup>

We now turn to the surface problem. As in the case of the  $d$ -wave pairing, boundary effects can also be expected for  $p$ -wave pairing.<sup>28,29)</sup> Due to the boundary condition eq. (2.11) the gap equation (2.14) shows  $\Delta_x=0$  at  $x=0$ . This is related to the fact that the sign of the  $p_x$ -wave order parameter changes after the reflection at the surface. In Fig. 2 we show the self-consistently obtained order

parameter, the current density, the magnetic field and the vector potential. In the bulk region  $\Delta_x$  and  $\Delta_y$  take the same magnitude as expected. Even if we start from an arbitrary relative phase, it finally becomes  $\pm\pi/2$  yielding the  $p_x \pm ip_y$ -wave state. In the GL theory this effect is included in the following fourth order term of the GL free energy which is derived in the Appendix,

$$A_4 \left[ 2|\Delta_x|^2 |\Delta_y|^2 + \frac{1}{2} (\Delta_x^2 \Delta_y^{*2} + \Delta_x^{*2} \Delta_y^2) \right]. \quad (3.4)$$

The first term represents the competition between  $\Delta_x$  and  $\Delta_y$ , while the second term favors  $\pm\pi/2$  for their relative phase. Since the coefficient of the first term is four times larger than the second one,  $p_x$ - and  $p_y$ -waves have to compete anyway. Near the boundary  $\Delta_y$  is enhanced as shown in Fig. 2(a). This enhancement is connected with the suppression of  $\Delta_x$  near the surface, which opens the way for  $\Delta_y$  to appear as a “single” order parameter. However, we find that  $\Delta_y$  at the boundary (about 1.24) is larger than  $\Delta_{\text{single}}(0)$  ( $\Delta_{\text{single}}(0)/\Delta(0) \simeq 1.21$ ). Note that similar enhancement also appears in  $d$ -wave superconductors.<sup>33,24)</sup> The reason can be seen in the following sixth order term of the GL free energy,

$$-4A_6 |\Delta_y|^2 |D_x \Delta_x|^2. \quad (3.5)$$

This term supports the  $\Delta_y$ -component whenever  $\Delta_x$  has a spatial variation and explains why  $\Delta_y > \Delta_{\text{single}}$  near the surface. Microscopically the enhancement of  $\Delta_y$  near the surface originates from the enhanced local density of states due to additional (bound) states appearing at low energy close to the surface as a result of the depletion of  $\Delta_x$  (as we will see below). Obviously only the  $p_y$ -component can benefit from this additional density of states near the Fermi energy, since it does not suffer from pair breaking for the surface perpendicular to the  $x$ -axis.

Due to the broken time-reversal symmetry, the local current flows along the surface as shown in Fig. 2(b), whose direction is reversed if we change the relative phase of the order parameter components ( $p_x + ip_y \leftrightarrow p_x - ip_y$ ) (time reversal operation). The current along the  $x$ -direction is zero as expected. The magnetic field is induced by the surface current and it is screened by the Meissner effect, so that the total current becomes zero.<sup>42)</sup> Note that depending on the geometry of the sample these currents can generate a finite magnetization.

### 3.2 Density of states

Due to the pair breaking effects we expect a modification of the local density of states near the boundary. The Andreev reflection and the conductance for the triplet pairing states were studied previously by various groups that the features of the conductance peak, which are related to the bound states, depend strongly on the angle of the incidence.<sup>28,29)</sup> The angle-resolved tunneling spectroscopy is related to the local density of states for a fixed Fermi momentum which is obtained from the quasi-classical Green function,

$$N(\theta_k, E, x) = \text{Re} \left[ g(\theta_k, \omega_m, x) \Big|_{i\omega_m \rightarrow E+i\delta} \right], \quad (3.6)$$

where  $\delta$  is a positive infinitesimal real number. Before examining the self-consistent order parameters case, it is illustrative to start with the consideration of a uniform order parameter, neglecting also the vector potential. In this case we can obtain the quasi-classical Green function analytically,<sup>33,24)</sup>

$$\begin{aligned}
\hat{g}(\theta_k, \omega_m, x) &= g_x(\theta_k, \omega_m, x)\hat{\tau}_x + g_y(\theta_k, \omega_m, x)\hat{\tau}_y + g_z(\theta_k, \omega_m, x)\hat{\tau}_z, \\
g_x(\theta_k, \omega_m, x) &= g_x(\pi - \theta_k, \omega_m, x) = \frac{-\Delta_y(\theta_k)}{\Omega} \left[ 1 + \frac{\Delta_x^2(\theta_k)}{\omega_m^2 + \Delta_y^2(\theta_k)} e^{-2qx} \right] - i \frac{\omega_m |\Delta_x(\theta_k)|}{\omega_m^2 + \Delta_y^2(\theta_k)} e^{-2qx}, \\
g_y(\theta_k, \omega_m, x) &= -g_y(\pi - \theta_k, \omega_m, x) = \frac{-\Delta_x(\theta_k)}{\Omega} \left[ 1 - e^{-2qx} \right], \\
g_z(\theta_k, \omega_m, x) &= g_z(\pi - \theta_k, \omega_m, x) = \frac{\omega_m}{\Omega} + \frac{\omega_m \Delta_x^2(\theta_k) - i\Omega |\Delta_x(\theta_k)| \Delta_y(\theta_k)}{\Omega [\omega_m^2 + \Delta_y^2(\theta_k)]} e^{-2qx}, \\
\Delta_x(\theta_k) &= \Delta(T) \cos \theta_k, \quad \Delta_y(\theta_k) = \Delta(T) \sin \theta_k, \quad \Omega = \sqrt{\omega_m^2 + \Delta^2(T)}, \quad q = \frac{\Omega}{|v_{Fx}|}.
\end{aligned} \tag{3.7}$$

Here  $\hat{\tau}_i$  ( $i=x, y, z$ ) is the Pauli matrix in the charge space. We have assumed  $p_x+ip_y$ -wave symmetry, i.e.  $\Delta(\theta_k)=\Delta_x(\theta_k)+i\Delta_y(\theta_k)=\Delta(T)(\cos \theta_k+i\sin \theta_k)$ , where  $\Delta(T)$  is the magnitude of the order parameter in the bulk region at temperature  $T$ . At low temperatures we obtain  $\Delta(T)\simeq\Delta(0)$ . Note that the enhancement of  $\Delta_y$  near the boundary in Fig. 2(a) can be understood by the first term of  $g_x$

$$\Delta_y(\theta_k) \left[ 1 + \frac{\Delta_x^2(\theta_k)}{\omega_m^2 + \Delta_y^2(\theta_k)} e^{-2qx} \right] > \Delta_y(\theta_k). \tag{3.8}$$

The vanishing of  $\Delta_x$  at the boundary can be derived from the equation for  $g_y$ . Substituting  $g_z$  into eq. (3.6), we have the following expression for the local density of states,

$$\begin{aligned}
N(\theta_k, E, x) &= N(\pi - \theta_k, E, x) \\
&= \left[ \frac{|E|}{\rho} - \frac{\Delta_x^2(\theta_k) |E| \cos(2\eta x) + \text{sgn}(E) |\Delta_x(\theta_k)| \Delta_y(\theta_k) \rho \sin(2\eta x)}{\rho [E^2 - \Delta_y^2(\theta_k)]} \right] \theta(E^2 - \Delta^2(T)) \\
&\quad + \pi |\Delta_x(\theta_k)| \exp\left(-\frac{2|\Delta_x(\theta_k)|}{|v_{Fx}|} x\right) \delta(E - \Delta_y(\theta_k)), \\
\rho &= \sqrt{E^2 - \Delta^2(T)}, \quad \eta = \frac{\rho}{|v_{Fx}|}.
\end{aligned} \tag{3.9}$$

The first term of eq. (3.9) represents the continuum quasiparticle states, while the second term describes the bound state. For  $\Delta_y=0$  the bound state is located at  $E=0$  while a finite  $p_y$ -wave part leads to  $E=\Delta_y(\theta_k)=\Delta(T) \sin \theta_k$ .<sup>28)</sup> This breaks the symmetry with respect to  $k_y \rightarrow -k_y$ , so that the quasiparticle bound states with positive and negative  $k_y$  have different occupation at low temperatures. Consequently, the quasiparticles generate a finite local surface current flows. For the uniform order parameter it is easy to see that  $J_y(x)$  has a finite value at  $x=0$  due to the  $|\Delta_x|\Delta_y$  term of  $g_z$  in eq. (3.7), at  $T=0$   $J_y(0)=ev_F N(0)\frac{1}{2}\Delta(0)$ . This shows that the number of quasiparticles contributing to the current is of the order of  $N(0)\Delta(0)$ .

We now turn to the results of the full selfconsistent calculation. Figure 3 shows the local density of states for a fixed momentum  $k_y>0$  ( $\theta_k=\pi/8$ ) from the self-consistently determined order



parameter and vector potential. The energy of the bound state estimated from eq. (3.9) is  $\sin(\pi/8)\Delta(T)\simeq 0.38\Delta(T)$ . In the  $k_y < 0$  case this energy is reversed in sign, since  $g$  has the symmetry of eq. (2.7). Therefore the integrated density of states over the Fermi surface is symmetric under  $E \rightarrow -E$ . In the case of the uniform order parameters the total local density of states at the boundary exactly becomes the same as the normal state, i.e. constant. One can test this by integrating eq. (3.9) over  $\theta_k$  at  $x=0$ . We show the local density of states calculated from eq. (3.9) in Figs. 4(a) and (b). When we move away from the boundary, the bound states rapidly decreases and the bulk property is recovered.

On the other hand, we notice gap structures in Fig. 4(d) even at  $x=0$  for the self-consistent order parameter. At the surface we can see two gap energies, one is  $E/\Delta(T)\simeq 1$ , and the other forms a double peak feature around about 1.25. The first one corresponds to the bulk gap energy, while the second one is identified as the magnitude of  $\Delta_y$  at  $x=0$ , which is enhanced near the boundary. These higher energy peaks are mainly formed by quasiparticles moving almost parallel to the surface as shown in Fig. 5(a), since they experience the enhanced  $\Delta_y$  over a long distance (see Fig. 5(b)). According to eq. (2.4) the energy should be replaced by  $E \rightarrow E - ev_{Fy}A_y$  in the presence of a vector potential. This yields an energy shift in the density of states. Quasiparticles running almost parallel to the surface are strongly affected by the vector potential due to the factor  $v_{Fy}A_y$ . Without the vector potential, the higher energy peaks merge into a single peak. Hence, the vector potential leads to the splitting into two peaks corresponding to the left and right moving particles along the surface. On the other hand, the bound states are mainly formed by the quasiparticle moving almost perpendicular to the surface shown in Figs. 5(c) and (d), which are only weakly affected by the vector potential. The self-consistently determined  $\Delta_x$  shows a continuous spatial change near the surface which leads to a reduction of the magnitude of the delta function peak corresponding to the bound state in  $N(\theta_k, E, x)$  compared to the uniform order parameter case. The reason is the widening of the potential well in which the bound state quasiparticle is trapped. The spatial dependence of  $\Delta_x$  can be approximately expressed by  $\tanh(x/(rv_F/\Delta(T)))$ , where  $r$  controls the decay length of  $\Delta_x$ . The magnitude of the bound state is then estimated by<sup>24)</sup>

$$I(r) = \frac{\Gamma(r + 1/2)}{\Gamma(1/2)\Gamma(1 + r)}. \quad (3.10)$$

Here  $\Gamma$  is the gamma function, and  $I(r)$  takes 1 for  $r=0$  and decreases with the increase of  $r$ . For the self-consistent order parameter  $r$  and  $I(r)$  can be estimated as 1 and 0.5, respectively. Therefore the density of states of the bound state at  $x=0$  in Fig. 4(d) is about half of Fig. 4(b).

Consequently, the local density of states near the boundary is sensitive to the spatial dependence of the order parameter, so that the self-consistent treatment is needed for quantitative discussions. However, the approximation of the uniform order parameters is helpful to capture the essence of the boundary effect.

#### §4. External Magnetic Field

In this section we study properties of the surface in an applied external magnetic field  $B_{\text{ext}}$  to the  $p_x+ip_y$ -wave state. In this case the boundary condition for the magnetic field is  $B_z(0)=B_{\text{ext}}$ , so that the first equation of (2.16) has to be replaced by

$$B_z(x) = B_{\text{ext}} - \mu \int_0^x dx' J_y(x'). \quad (4.1)$$

We show the results of the self-consistent solution in Fig. 6. The order parameter does not suffer a significant modification compared with the situation without the external field. In Fig. 6(d) we can see that the peak position, which corresponds to the enhanced  $\Delta_y$ , shifts in a higher (lower) energy region if we apply a negative (positive) field to the surface. The peak mainly comes from the quasiparticle having momentum of  $\theta_k \simeq \pi/2$  as discussed before, which acquire an energy shift  $-ev_{\text{F}y}A_y$ . In the case of negative  $B_{\text{ext}}$ , there is an additional positive contribution to the vector potential which shifts the peak related to the gap towards higher energies. If  $B_{\text{ext}}$  is reversed, the vector potential decreases and is almost zero at the surface when  $B_{\text{ext}}=0.1B_C$ . Then the two peaks merge into a single peak as shown in Fig. 6(d). Increasing the external field further in the positive direction, the vector potential is reversed (see Fig. 6(c)), so that the peak splits again. The lines A and B in Fig. 6(d) correspond to the peak with the positive and negative  $k_y$ , respectively. Energetically the case of the negative field is expected to be stable as it further opens the gap.

In the  $d$ -wave case bound states are located at  $E=0$ ,<sup>21)</sup> so that the peak structure at the zero energy is split by the vector potential.<sup>43)</sup> In the present  $p_x \pm ip_y$ -wave case bound states distribute inside the energy gap and form an almost flat local density of states at the surface as shown in Fig. 4(d). Near zero energy the shift is small due to the small  $v_{\text{F}y}$  factor, since the states near zero energy are formed by the quasiparticles having momenta of  $\theta_k \ll \pi/2$ . Therefore the energy shift due to an external field is not observable for energies below the gap. The gap structure sensitive to the applied external magnetic field is located rather at energies corresponding to the enhanced  $\Delta_y$  at the surface.

#### §5. Domain Wall

A modified quasiparticle spectrum is also expected near the domain wall. Clearly, domain walls cost energy and are not desirable modification of the order parameter. However, they exist even at low temperatures, since once they have formed at the onset of superconductivity, they are easily pinned at defects in the material and cannot move out of the sample. Domain walls between the pinning centers may give good targets for scanning tunneling spectroscopy on the sample surface. Physical properties of domain walls in unconventional superconductors have been investigated in the framework of the GL theory.<sup>38,39)</sup> Here we investigate their quasiparticle properties within the quasi-classical approximation which is essential for the tunneling spectroscopy. We will not examine effects of the external magnetic field in this case, because the magnetic field would not reach the

domain wall due to the Meissner screening.

There are two kinds of domain walls separating the two degenerate superconducting states. For the domain wall perpendicular to the  $x$ -axis we have the  $(p_x - ip_y | p_x + ip_y)$  structure and the  $(-p_x + ip_y | p_x + ip_y)$  structure, i.e. one of the two order parameter components should change sign at the domain wall. From the GL formulation it is expected that the first type is more stable, since the gradient free energy of the  $p_x$ -wave is three times larger than that of  $p_y$ -wave (see  $F_4^{\text{grad}}$  in eq. (A.11)).

We assume that there is no scattering at the domain wall leading to quasi-classical trajectories as shown in Fig. 7. The boundary condition for the domain wall case is also given by eq. (2.11) with  $\mathbf{k}_{F1} = \mathbf{k}_{F2}$ . In the domain wall case  $J_y(x)$  is symmetric under the  $x \rightarrow -x$  transformation. Therefore the vector potential is also symmetric and the magnetic field becomes anti-symmetric.

### 5.1 The $(p_x - ip_y | p_x + ip_y)$ domain wall

In Fig. 8 we show the results of the self-consistent solution. A current is induced near the domain wall and it is screened due to the Meissner effect.<sup>39)</sup> Figure 8(a) shows that the relative phase between the  $p_x$ - and  $p_y$ -wave component suddenly changes, if we go through the domain wall (type I). On the other hand, the relative phase can change continuously, approximately as  $\frac{\pi}{2} \tanh(x/r\xi_0)$  (type II). These two types were discussed previously within the GL formulation.<sup>38,39)</sup> In the case of type II domain walls the relative phase changes gradually from  $+\pi/2$  to  $-\pi/2$ . Our calculation shows that the type I solution is energetically favored for the cylindrical symmetry Fermi surface case.

Despite several similarities with the order parameter structure between the surface and the domain wall, there are important differences in the quasiparticle spectrum as seen by comparing Figs. 4(d) and 8(d). In Fig. 4(d) a gap structure can be seen at  $E/\Delta(T) \simeq 1.25$ , while there is no gap feature at the corresponding energy in Fig.8(d). In Fig. 9 we show the schematic spatial dependence of the self-consistent order parameters, which a quasiparticle encounters along the classical trajectory. As we mentioned in §3, the higher energy peak for the surface case is mainly formed by the quasiparticles which run almost parallel to the surface. The same situation occurs also in the domain wall case, where the quasiparticle with momentum  $\theta_k \simeq 0$  mainly contribute to the gap structure. Compared to the surface cases the distance in which the quasiparticle experiences the enhanced order parameter  $\Delta_x$  is short (see Fig. 9(b)), so that the gap structure does not appear in the  $(p_x - ip_y | p_x + ip_y)$  domain wall case.

There is another characteristic point in Fig. 8(d), a small gap near the zero energy. The density of states near the zero energy mainly comes from the region where  $\theta_k \simeq \pi/2$  for the domain wall case (see Figs. 9(c) and (d)). The vector potential can generate a shift of the energy towards higher values. In the  $\theta_k \simeq \pi/2$  case the magnitude of the shift can be estimated as  $ev_F A_y(0) \simeq 0.1$ , which is shown in Fig. 8(b). The small gap in Fig. 8(d) is about 0.1, which is consistent to this estimate.

In fact, neglecting the vector potential, we find that the gap structure in the small energy region has disappeared.

A further difference from the surface case is the v-shaped density of states below the bulk energy gap. The origin of this feature is the gradual spatial dependence of  $\Delta_y \sin \theta_k$  on the classical trajectory with  $\theta_k \simeq \pi/2$  (see Fig. 9(d)), which gives rise to additional bound states close to the bulk gap energy,<sup>24)</sup> so that the density of states at low energies is shifted up to higher energy region.

### 5.2 The $(-p_x + ip_y | p_x + ip_y)$ domain wall

In this case the system also favors the type I behavior for the relative phase. Here the situation is very similar to the surface case. (In the surface case  $\Delta_x$  changes its sign after the reflection at surface.) Therefore most of the properties are the same and differences between them appear only on the Fermi wave length scale.

If the Fermi surface is not cylindrical, then the properties of the domain walls can be modified and a type II domain wall may be realized in some cases.<sup>39)</sup>

## §6. Summary

In this paper we analyzed the properties of the order parameter and the quasiparticles of a  $p_x \pm ip_y$ -wave superconductor near the surface and at a domain wall. For this purpose we used a quasiclassical approximation which allows us to determine selfconsistently the current density, magnetic field and vector potential distribution besides the order parameter.

The spatial dependence of the order parameter at the surface shows a suppression for the component  $\mathbf{p} \parallel \mathbf{n}$  where  $\mathbf{n}$  is the surface normal vector, i.e. the  $p_x$ -component is suppressed for the surface perpendicular to  $x$ -axis. The perpendicular component, on the other hand, is slightly enhanced. In the surface region we found bound states whose energy strongly depends on the position of the quasiparticle momentum on the Fermi surface. The average over the Fermi surface shows that this bound state yields a density of states which is essentially constant within the gap at the surface. As we move towards the bulk region these bound states gradually disappear and the complete bulk gap is recovered. We have also demonstrated that an external field (parallel to the  $c$ -axis) modifies the local density of states differently for the two degenerate states. Similar to the case of the time reversal symmetry breaking surface of the  $d$ -wave superconductor we find that the bound states carry a spontaneous current whose direction is opposite for the two degenerate superconducting bulk states. Furthermore an external magnetic field modifies the local density of states at the surface significantly only for energies slightly above the bulk energy gap, while the subgap state structure is essentially unaffected.

The domain wall shows various similarities with the surface. One order parameter component is suppressed while the other is slightly enhanced. In contrast to the situation at surface, however, the suppressed and enhanced components are the ones with  $\mathbf{p} \perp \mathbf{n}$  and  $\mathbf{p} \parallel \mathbf{n}$ , respectively, which yields

the narrower (energetically more favorable) domain wall than in the opposite case. At the surface the choice is not available since the role of the order parameter components is entirely determined by the boundary condition due to the surface scattering. There are, in principle, two types of domain walls: In the type I domain wall the suppressed order parameter component vanishes in the center of the domain wall. For the type II domain wall this component introduces a phase twist which yields a finite modulus everywhere. The latter domain wall state is two-fold degenerate. The calculation using a cylindrical Fermi surface showed that the type I domain wall is more stable at all temperatures. This would change, if, for example, the anisotropy of the Fermi surface is taken into account.

The local density of states in the center of the type I domain wall shows a tiny gap, while the structure of the large bulk gap remains visible. The shift of density of states is due to the presence of bound states in the domain wall similar to the surface and the tiny gap is a feedback effect of the vector potential created by the quasiparticles themselves. This change of the density of states could provide a possible way to detect domain walls by scanning tunneling microscopy. For a given voltage within the bulk gap the scanning of the (*c*-axis oriented) sample surface would yield an enhanced current in the region close to the domain wall.

Analogous to the surface case the bound states in the domain wall carry a spontaneous current which yields a magnetic field distribution. In contrast to the surface the net magnetization generated by these currents at the domain wall has to be zero, since inside the superconductor magnetic flux can only enter in form of vortices enclosing a fixed quantum of flux. Thus, the magnetic fields of the domain walls are invisible on a macroscopic level. Even a scanning SQUID microscope has, at present, still too little spatial resolution to observe these fields.

For the cylindrical Fermi surface the properties of the domain wall and the surface do not depend on the orientation of the normal vector as long as it lies within the *x-y*-plane. The real superconductor has certainly an anisotropic Fermi surface which could change various properties of the quasiparticle states for both the surface and the domain wall. To what degree changes occur remains a problem for future studies.

## Acknowledgments

One of the authors (M. M.) expresses his sincere thanks to Prof. H. Shiba for his critical reading of the manuscript. We are grateful to Dr. S. Higashitani and Prof. K. Nagai for pointing out the correct expression of the current density. We would like to thank also Dr. Y. Okuno for many helpful discussions. This work was supported by Grant-in-Aid for Scientific Research from the Ministry of Education, Science and Culture, Japan.

## Appendix: Ginzburg-Landau Free Energy

In §3 we have shown that the self-consistent order parameters favor the time-reversal symmetry breaking state ( $p_x \pm i p_y$ -wave), and that the  $p_y$ -wave part is enhanced by the presence of the  $p_x$ -wave. In order to understand these results from a different point of view, we derive the GL free energy. The GL free energy can be easily derived by using the quasi-classical Green function.<sup>44)</sup> For simplicity the vector potential is neglected here.

To derive the GL free energy, let us rewrite eq. (2.6) in the following form:

$$\begin{aligned}\omega_m f(\mathbf{k}_F, \omega_m, x) &= \Delta(\mathbf{k}_F, x) g(\mathbf{k}_F, \omega_m, x) - D f(\mathbf{k}_F, \omega_m, x), \\ \omega_m \bar{f}(\mathbf{k}_F, \omega_m, x) &= \Delta^*(\mathbf{k}_F, x) g(\mathbf{k}_F, \omega_m, x) + D \bar{f}(\mathbf{k}_F, \omega_m, x), \\ g^2(\mathbf{k}_F, \omega_m, x) &= 1 - f(\mathbf{k}_F, \omega_m, x) \bar{f}(\mathbf{k}_F, \omega_m, x),\end{aligned}\tag{A.1}$$

where  $D = \frac{v_{Fx}}{2} \frac{\partial}{\partial x}$  and we have assumed the system is uniform in the  $y$  direction, i.e. there is no  $y$  dependence in  $g$ ,  $f$  and  $\bar{f}$ .  $\Delta(\mathbf{k}_F, x)$  is assumed to be composed of  $p_x$ - and  $p_y$ -waves. Since we are interested in the temperature near  $T_C$ , the order parameters are assumed to be small. The gradient term ( $D$  term) can be expressed as

$$\frac{D}{T} \sim \frac{|v_{Fx}|}{T_C} \frac{\partial}{\partial x} \sim \frac{|v_{Fx}|}{\Delta(0)} \frac{\partial}{\partial x} \sim \frac{\partial}{\partial(x/\xi_0)},\tag{A.2}$$

where  $\xi_0 = v_F/\pi\Delta(0)$ , which is the coherence length at  $T=0$ . For  $T \rightarrow T_C$ , the spatial dependence of the order parameter is of the order of  $\xi(T) \sim v_F/\pi\Delta(T)$ , and  $D/T \sim O(\Delta/T) \ll 1$ . Let us treat  $\Delta/T$  as a perturbation and derive the functions  $f$ ,  $\bar{f}$  and  $g$  in a power series of  $\Delta/T$ ,

$$\begin{aligned}f &= f_0 + f_1 + f_2 + \dots, \\ \bar{f} &= \bar{f}_0 + \bar{f}_1 + \bar{f}_2 + \dots, \\ g &= g_0 + g_1 + g_2 + \dots,\end{aligned}\tag{A.3}$$

where the subscripts represent the order of  $\Delta/T$ . The lowest order is contained in the bulk solution

$$f_{\text{bulk}} = \frac{\Delta}{\sqrt{\omega_m^2 + |\Delta|^2}}, \quad \bar{f}_{\text{bulk}} = \frac{\Delta^*}{\sqrt{\omega_m^2 + |\Delta|^2}}, \quad g_{\text{bulk}} = \frac{\omega_m}{\sqrt{\omega_m^2 + |\Delta|^2}}.\tag{A.4}$$

Therefore the zeroth order functions are given by

$$f_0 = 0, \quad \bar{f}_0 = 0, \quad g_0 = \frac{\omega_m}{|\omega_m|}.\tag{A.5}$$

Since  $f$  and  $\bar{f}$  are related to the order parameter, they do not have the zeroth order term. We can obtain the functions  $f$ ,  $\bar{f}$  and  $g$  up to any order of  $\Delta/T$  by using eqs. (A.1) and (A.5).<sup>44)</sup> The results are as follows:

$$\begin{cases} f_1 = \frac{\Delta}{|\omega_m|}, \\ \bar{f}_1 = \frac{\Delta^*}{|\omega_m|}, \\ g_1 = 0, \end{cases}$$

$$\begin{cases}
f_2 = -\frac{D\Delta}{\omega_m|\omega_m|}, \\
\bar{f}_2 = \frac{D\Delta^*}{\omega_m|\omega_m|}, \\
g_2 = -\frac{|\Delta|^2}{2\omega_m|\omega_m|}, \\
f_3 = \frac{-\Delta|\Delta|^2/2+D^2\Delta}{\omega_m^2|\omega_m|}, \\
\bar{f}_3 = \frac{-\Delta^*|\Delta|^2/2+D^2\Delta^*}{\omega_m^2|\omega_m|}, \\
g_3 = \frac{-\Delta D\Delta^*+\Delta^*D\Delta}{2\omega_m^2|\omega_m|}. \\
f_4 = \frac{(-\Delta^2 D\Delta^*+|\Delta|^2 D\Delta)/2+D\Delta|\Delta|^2/2-D^3\Delta}{\omega_m^3|\omega_m|}, \\
\bar{f}_4 = \frac{(\Delta^{*2} D\Delta-|\Delta|^2 D\Delta^*)/2-D\Delta^*|\Delta|^2/2+D^3\Delta^*}{\omega_m^3|\omega_m|}, \\
g_4 = \frac{3|\Delta|^4/4-\Delta D^2\Delta^*-\Delta^*D^2\Delta+(D\Delta)(D\Delta^*)}{2\omega_m^3|\omega_m|}, \\
f_5 = \frac{\Delta \left[ 3|\Delta|^4/4-\Delta D^2\Delta^*-\Delta^*D^2\Delta+(D\Delta)(D\Delta^*) \right] - D \left[ -\Delta^2 D\Delta^*+|\Delta|^2 D\Delta+D\Delta|\Delta|^2-2D^3\Delta \right]}{2\omega_m^4|\omega_m|}, \\
\bar{f}_5 = \frac{\Delta^* \left[ 3|\Delta|^4/4-\Delta^* D^2\Delta-\Delta D^2\Delta^*+(D\Delta^*)(D\Delta) \right] - D \left[ -\Delta^{*2} D\Delta+|\Delta|^2 D\Delta^*+D\Delta^*|\Delta|^2-2D^3\Delta^* \right]}{2\omega_m^4|\omega_m|},
\end{cases} \tag{A.6}$$

The gap equation can be written by using  $f$  and  $\bar{f}$  as

$$\begin{pmatrix} \Delta_x(x) \\ \Delta_y(x) \end{pmatrix} = 2\pi V_p T \sum_{0 < \omega_m < \omega_C} \frac{1}{2\pi} \int_{-\pi}^{\pi} d\theta_k \begin{pmatrix} 2 \cos(\theta_k) \\ 2 \sin(\theta_k) \end{pmatrix} \left[ f(\theta_k, \omega_m, x) + \bar{f}^*(\theta_k, \omega_m, x) \right]. \tag{A.7}$$

Substituting  $f$  and  $\bar{f}$  up to the fifth order into eq. (A.7), we obtain the gap equation for the  $p_x$ -wave

$$\begin{aligned}
& -A_2\Delta_x + A_4 \left[ 3\Delta_x|\Delta_x|^2 + 2\Delta_x|\Delta_y|^2 + \Delta_x^*\Delta_y^2 \right] - 6A_4D_x^2\Delta_x \\
& -\frac{3}{4}A_6 \left[ 5\Delta_x|\Delta_x|^4 + \Delta_x^3\Delta_y^{*2} + 6\Delta_x|\Delta_x|^2|\Delta_y|^2 + 3\Delta_x^*|\Delta_x|^2\Delta_y^2 + 3\Delta_x|\Delta_y|^4 + 2\Delta_x^*|\Delta_y|^2\Delta_y^2 \right] \\
& + 5A_6 \left[ \Delta_x^2D_x^2\Delta_x^* + 2\Delta_x|D_x\Delta_x|^2 + 3\Delta_x^*(D_x\Delta_x)^2 + 4|\Delta_x|^2D_x^2\Delta_x \right] - 10A_6D_x^4\Delta_x \\
& + A_6 \left[ 2\Delta_x\Delta_yD_x^2\Delta_y^* + 4\Delta_x\Delta_y^*D_x^2\Delta_y + 2\Delta_x|D_x\Delta_y|^2 + 4\Delta_x^*\Delta_yD_x^2\Delta_y + 3\Delta_x^*(D_x\Delta_y)^2 + \Delta_y^2D_x^2\Delta_x^* \right. \\
& \quad \left. + 4|\Delta_y|^2D_x^2\Delta_x + 2\Delta_y(D_x\Delta_x)(D_x\Delta_y^*) + 2\Delta_y(D_x\Delta_y)(D_x\Delta_x^*) + 6\Delta_y^*(D_x\Delta_x)(D_x\Delta_y) \right] = 0, \\
A_2 = 1 - \frac{T}{T_C}, \quad A_4 = \frac{1}{4} \frac{7}{8} \frac{\zeta(3)}{(\pi T)^2}, \quad A_6 = \frac{1}{8} \frac{31}{32} \frac{\zeta(5)}{(\pi T)^4}, \quad D_x = \frac{1}{2} v_F \frac{\partial}{\partial x},
\end{aligned} \tag{A.8}$$

and for the  $p_y$ -wave

$$\begin{aligned}
& -A_2\Delta_y + A_4 \left[ 3\Delta_y|\Delta_y|^2 + 2\Delta_y|\Delta_x|^2 + \Delta_y^*\Delta_x^2 \right] - 2A_4D_x^2\Delta_y \\
& -\frac{3}{4}A_6 \left[ 5\Delta_y|\Delta_y|^4 + \Delta_y^3\Delta_x^{*2} + 6\Delta_y|\Delta_y|^2|\Delta_x|^2 + 3\Delta_y^*|\Delta_y|^2\Delta_x^2 + 3\Delta_y|\Delta_x|^4 + 2\Delta_y^*|\Delta_x|^2\Delta_x^2 \right] \\
& + A_6 \left[ \Delta_y^2D_x^2\Delta_y^* + 2\Delta_y|D_x\Delta_y|^2 + 3\Delta_y^*(D_x\Delta_y)^2 + 4|\Delta_y|^2D_x^2\Delta_y \right] - 2A_6D_x^4\Delta_y \\
& + A_6 \left[ 2\Delta_y\Delta_xD_x^2\Delta_x^* + 4\Delta_y\Delta_x^*D_x^2\Delta_x + 2\Delta_y|D_x\Delta_x|^2 + 4\Delta_y^*\Delta_xD_x^2\Delta_x + 3\Delta_y^*(D_x\Delta_x)^2 + \Delta_x^2D_x^2\Delta_y^* \right. \\
& \quad \left. + 4|\Delta_x|^2D_x^2\Delta_y + 2\Delta_x(D_x\Delta_y)(D_x\Delta_x^*) + 2\Delta_x(D_x\Delta_x)(D_x\Delta_y^*) + 6\Delta_x^*(D_x\Delta_y)(D_x\Delta_x) \right] = 0.
\end{aligned} \tag{A.9}$$

Here  $\zeta(z)$  is the Riemann zeta function. The GL free energy should recover the above gap equations

through the following Euler-Lagrange equation,

$$\left[ \frac{\partial}{\partial \Delta^*} - D_x \frac{\partial}{\partial (D_x \Delta^*)} + D_x^2 \frac{\partial}{\partial (D_x^2 \Delta^{*2})} \right] F = 0. \quad (\text{A}\cdot 10)$$

The result of the free energy density up to sixth order is as follows:

$$\begin{aligned} F &\propto F_2 + F_4 + F_6 + F_4^{\text{grad}} + F_{6a}^{\text{grad}} + F_{6b}^{\text{grad}} + F_{6c}^{\text{grad}}, \\ F_2 &= -A_2 \left[ |\Delta_x|^2 + |\Delta_y|^2 \right], \\ F_4 &= A_4 \left[ \frac{3}{2} (|\Delta_x|^4 + |\Delta_y|^4) + 2|\Delta_x|^2 |\Delta_y|^2 + \frac{1}{2} (\Delta_x^2 \Delta_y^{*2} + \Delta_x^{*2} \Delta_y^2) \right], \\ F_6 &= -A_6 \left[ \frac{5}{4} (|\Delta_x|^6 + |\Delta_y|^6) + \frac{9}{4} (|\Delta_x|^4 |\Delta_y|^2 + |\Delta_x|^2 |\Delta_y|^4) + \frac{3}{4} (|\Delta_x|^2 + |\Delta_y|^2) (\Delta_x^2 \Delta_y^{*2} + \Delta_x^{*2} \Delta_y^2) \right], \\ F_4^{\text{grad}} &= A_4 \left[ 6|D_x \Delta_x|^2 + 2|D_x \Delta_y|^2 \right], \\ F_{6a}^{\text{grad}} &= -A_6 \left\{ 20|\Delta_x|^2 |D_x \Delta_x|^2 + \frac{5}{2} \left[ \Delta_x^2 (D_x \Delta_x^*)^2 + \Delta_x^{*2} (D_x \Delta_x)^2 \right] \right. \\ &\quad \left. + 4|\Delta_y|^2 |D_x \Delta_y|^2 + \frac{1}{2} \left[ \Delta_y^2 (D_x \Delta_y^*)^2 + \Delta_y^{*2} (D_x \Delta_y)^2 \right] \right\}, \\ F_{6b}^{\text{grad}} &= -A_6 \left[ 10|D_x^2 \Delta_x|^2 + 2|D_x \Delta_y|^2 \right], \\ F_{6c}^{\text{grad}} &= -A_6 \left\{ \frac{1}{2} \left[ \Delta_x^2 (D_x \Delta_y^*)^2 + \Delta_x^{*2} (D_x \Delta_y)^2 + \Delta_y^2 (D_x \Delta_x^*)^2 + \Delta_y^{*2} (D_x \Delta_x)^2 \right] \right. \\ &\quad \left. + 2 \left[ \Delta_x \Delta_y (D_x \Delta_x^*) (D_x \Delta_y^*) + \Delta_x^* \Delta_y^* (D_x \Delta_x) (D_x \Delta_y) \right] \right. \\ &\quad \left. + 4 \left[ \Delta_x \Delta_y^* (D_x \Delta_x) (D_x \Delta_y^*) + \Delta_x^* \Delta_y (D_x \Delta_x^*) (D_x \Delta_y) \right] \right. \\ &\quad \left. + \Delta_x \Delta_y^* (D_x \Delta_x^*) (D_x \Delta_y) + \Delta_x^* \Delta_y (D_x \Delta_x) (D_x \Delta_y^*) + |\Delta_x|^2 |D_x \Delta_y|^2 + |\Delta_y|^2 |D_x \Delta_x|^2 \right\}. \end{aligned} \quad (\text{A}\cdot 11)$$

The coefficient of the free energy density is chosen to reproduce the well known bulk GL free energy. The terms which suppress the spatial change of the order parameters are  $6A_4|D_x \Delta_x|^2$  and  $2A_4|D_x \Delta_y|^2$  in the fourth gradient term. Therefore, the spatial variation of  $\Delta_x$  is energetically more expensive than that of  $\Delta_y$  along the  $x$ -direction. The asymmetry of the  $p_x$ - and  $p_y$ -waves comes from the  $D$  term, since  $D \propto v_{Fx} = v_F \cos \theta_k$ .  $F_{6a}^{\text{grad}}$  and  $F_{6b}^{\text{grad}}$  are the sixth order gradient free energies in which  $\Delta_x$  does not couple with  $\Delta_y$ , while  $F_{6c}^{\text{grad}}$  is the free energy in which the two components are coupled.

- 
- [1] Y. Maeno, H. Hashimoto, K. Yoshida, S. Nishizaki, T. Fujita, J. G. Bednorz and F. Lichtenberg: Nature **372** (1994) 532.
  - [2] A. P. Mackenzie, S. R. Julian, A. J. Diver, G. J. McMullan, M. P. Ray, G. G. Lonzarich and Y. Maeno: Phys. Rev. Lett. **76** (1996) 3786.
  - [3] T. Oguchi: Phys. Rev. B **51** (1995) 1385.
  - [4] D. J. Singh: Phys. Rev. B **52** (1995) 1358.
  - [5] K. Ishida, Y. Kitaoka, K. Asayama, S. Ikeda, S. Nishizaki, Y. Maeno, K. Yoshida and T. Fujita: Phys. Rev. B **56** (1997) R505.



- [6] A. P. Mackenzie, R. K. W. Haselwimmer, A. W. Tyler, G. G. Lonzarich, Y. Mori, S. Nishizaki and Y. Maeno: Phys. Rev. Lett. **80** (1998) 161.
- [7] T. M. Rice and M. Sigrist: J. Phys. Condens. Matter **7** (1995) L643.
- [8] G. Baskaran, Physica B **223 & 224** (1996) 490.
- [9] K. Machida, M. Ozaki and T. Ohmi: J. Phys. Soc. Jpn. **65** (1996) 3720.
- [10] M. Sigrist and M. E. Zhitomirsky: J. Phys. Soc. Jpn. **65** (1996) 3452.
- [11] I. I. Mazin and D. J. Singh: Phys. Rev. Lett. **79** (1997) 733.
- [12] T. C. Gibb, R. Greatrex, N. N. Greenwood, D. C. Puxley and K. G. Snowden: J. Solid State Chem. **11** (1994) 17.
- [13] M. Sigrist, K. K. Ng, A. Furusaki, D. Agterberg, C. Honerkamp, T. M. Rice and M. E. Zhitomirsky: Physica C **317-318** (1999) 134.
- [14] G. M. Luke, Y. Fudamoto, K. M. Kojima, M. I. Larkin, J. Merrin, B. Nachumi, Y. J. Uemura, Y. Maeno, Z. Q. Mao, Y. Mori, H. Nakamura and M. Sigrist: Nature **394** (1998) 558.
- [15] M. Sigrist, C. Honerkamp, D. Agterberg, T. M. Rice, M. E. Zhitomirsky and A. Furusaki: Physics and Chemistry of Transition-Metal Oxides (Proceedings of the 20th Taniguchi Symposium) Springer (1999).
- [16] K. Ishida, H. Mukuda, Y. Kitaoka, K. Asayama, Z. Q. Mao, Y. Mori and Y. Maeno: Nature **396** (1998) 658.
- [17] D. F. Agterberg, T. M. Rice and M. Sigrist: Phys. Rev. Lett. **78** (1997) 3374.
- [18] Y. Maeno, S. Nishizaki, K. Yoshida, S. Ikeda and T. Fujita: J. Low Temp. Phys. **105** (1996) 1577; S. Nishizaki, Y. Maeno, S. Farner, S. Ikeda and T. Fujita: Physica C **282-287** (1997) 1413; S. NishiZaki, Y. Maeno, S. Farner, S. Ikeda and T. Fujita: J. Phys. Soc. Jpn. **67** (1998) 560.
- [19] T. M. Riseman, P. G. Kealey, E. M. Forgan, A. P. Mackenzie, L. M. Galvin, A. W. Tyler, S. L. Lee, C. Ager, D. Mck. Paul, C. M. Aegerter, R. Cubitt, Z. Q. Mao, S. Akima and Y. Maeno: Nature **396** (1998) 242.
- [20] D. F. Agterberg: Phys. Rev. Lett. **80** (1998) 5184; D. F. Agterberg: Phys. Rev. B **58** (1998) 14484.
- [21] C. -R. Hu: Phys. Rev. Lett. **72** (1994) 1526; J. Yang and C. -R. Hu: Phys. Rev. B **50** (1994) 16766.
- [22] S. Kashiwaya, Y. Tanaka, M. Koyanagi, H. Takashima and K. Kajimura: Phys. Rev. B **51** (1995) 1350; Y. Tanaka and S. Kashiwaya: Phys. Rev. Lett. **74** (1995) 3451.
- [23] Y. Ohashi: J. Phys. Soc. Jpn. **64** (1995) 887; Y. Ohashi and S. Takada: J. Phys. Soc. Jpn. **65** (1996) 264; Y. Ohashi: J. Phys. Soc. Jpn. **65** (1996) 823.
- [24] M. Matsumoto and H. Shiba: J. Phys. Soc. Jpn. **64** (1995) 1703; *ibid.* 3384; *ibid.* 4867; *ibid.* **65** (1996) 2194.
- [25] Y. Nagato and K. Nagai: Phys. Rev. B **51** (1995) 16254; K. Yamada, Y. Nagato, S. Higashitani and K. Nagai: J. Phys. Soc. Jpn. **65** (1996) 1540.
- [26] L. J. Buchholtz, M. Palumbo, D. Rainer and J. A. Sauls: J. Low Temp. Phys. **101** (1995) 1079; *ibid.* 1099.
- [27] S. Higashitani: J. Phys. Soc. Jpn. **66** (1997) 2556.
- [28] C. Honerkamp and M. Sigrist: J. Low Temp. Phys. **111** (1998) 895.
- [29] M. Yamashiro, Y. Tanaka, Y. Tanuma and S. Kashiwaya: J. Phys. Soc. Jpn. **67** (1998) 3224.
- [30] N. Schopohl and K. Maki: Phys. Rev. B **52** (1995) 490; N. Schopohl: preprint.
- [31] M. Ichioka, N. Hayashi, N. Enomoto and K. Machida: Phys. Rev. B **53** (1996) 15316; M. Ichioka, N. Hayashi and K. Machida: Phys. Rev. B **55** (1997) 6565; N. Hayashi, M. Ichioka and K. Machida: Phys. Rev. B **56** (1997) 9052.
- [32] A. F. Andreev: Sov. Phys.-JETP. **19** (1964) 1228.
- [33] C. Bruder: Phys. Rev. B **41** (1990) 4017.
- [34] G. Eilenberger: Z. Physik **214** (1968) 195.
- [35] J. W. Serene and D. Rainer: Phys. Rep. **101** (1983) 221.

- [36] K. Nagai and J. Hara: J. Low Temp. Phys. **71** (1988) 351; *ibid* **72** (1988) 407; M. Ashida, S. Aoyama, J. Hara and K. Nagai: Phys. Rev. B **40** (1989) 8673; Y. Nagato and K. Nagai: J. Low Temp. Phys. **93** (1993) 33.
- [37] G. Kieselmann: Phys. Rev. B **35** (1987) 6762.
- [38] G. E. Volovik and L. P. Gor'kov: Sov. Phys.-JETP **61** (1985) 843.
- [39] M. Sigrist, T. M. Rice and K. Ueda: Phys. Rev. Lett. **63** (1989) 1727; M. Sigrist and K. Ueda: Rev. Mod. Phys. **63** (1991) 239.
- [40] Y. Nagato: Doctor thesis (Hiroshima Univ., 1994).
- [41] S. Higashitani and K. Nagai: J. Phys. Soc. Jpn. **64** (1995) 549.
- [42] Y. Ohashi and T. Momoi: J. Phys. Soc. Jpn. **65** (1996) 3254.
- [43] M. Fogelström, D. Rainer and J. A. Sauls: Phys. Rev. Lett. **79** (1997) 281; M. Covington, M. Aprili, E. Paraoanu and L. H. Greene: Phys. Rev. Lett. **79** (1997) 277.
- [44] N. Schopohl and L. Tewordt: J. Low Temp. Phys. **41** (1980) 305.

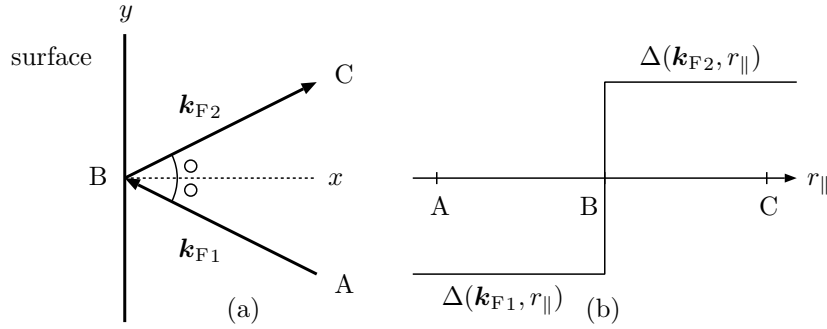


Fig. 1. (a) Classical trajectory of a quasiparticle, in which the momentum of the incident and reflected quasiparticles along the surface is conserved.  $\mathbf{k}_{F1}$  and  $\mathbf{k}_{F2}$  are the momentum with  $k_{Fx} < 0$  and  $k_{Fx} > 0$ , respectively. (b)  $r_{\parallel}$  is taken along the classical trajectory.  $\Delta(\mathbf{k}_{F1}, r_{\parallel})$  and  $\Delta(\mathbf{k}_{F2}, r_{\parallel})$  are the order parameters for the incident and reflected quasiparticles, respectively. A schematic spatial dependence is plotted.

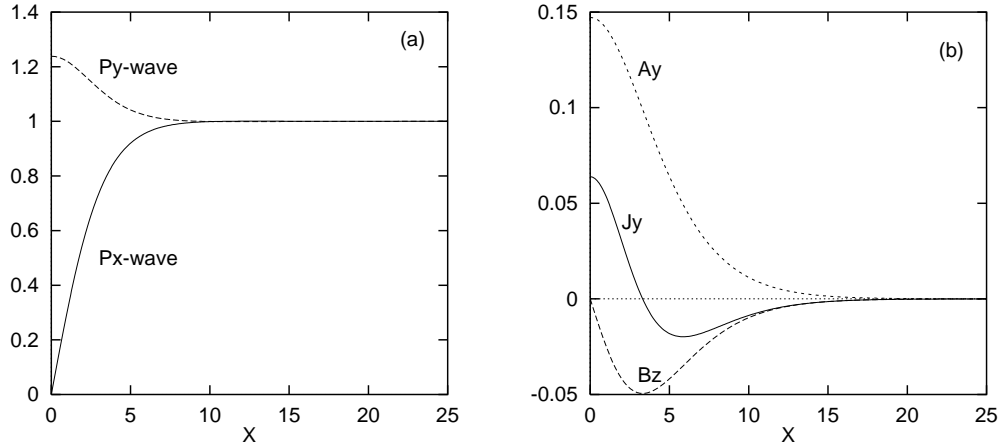


Fig. 2. (a) Spatial dependence of the self-consistent order parameters for  $p_x$ - and  $p_y$ -waves. They are scaled by the bulk value  $\Delta(T)$ . The  $x$  coordinate is also scaled by  $\xi_0 = v_F / \pi \Delta(0)$ , where  $\Delta(0)$  is the magnitude of the bulk order parameter at  $T=0$ .  $\Delta_x$  and  $\Delta_y$  are real and imaginary, respectively. The set of parameters are chosen as  $T=0.2T_C$ ,  $\omega_C=10T_C$ ,  $\kappa=\lambda_L/\xi_0=2.5$  (see ref. 19). Here  $\lambda_L = \sqrt{m/e^2\mu n}$  is the London penetration depth. (b) The self-consistent current density  $J_y(x)$ , magnetic field  $B_z(x)$  and vector potential  $A_y(x)$ . They are scaled by  $J_0 = ev_F N(0)T_C$ ,  $B_C = \Phi_0 / 2\sqrt{2}\pi\xi_0\lambda_L$  and  $\Delta(0)/ev_F$ , respectively. Here  $B_C$  and  $\Phi_0 = h/2e$  are the critical magnetic field and flux quantum, respectively.

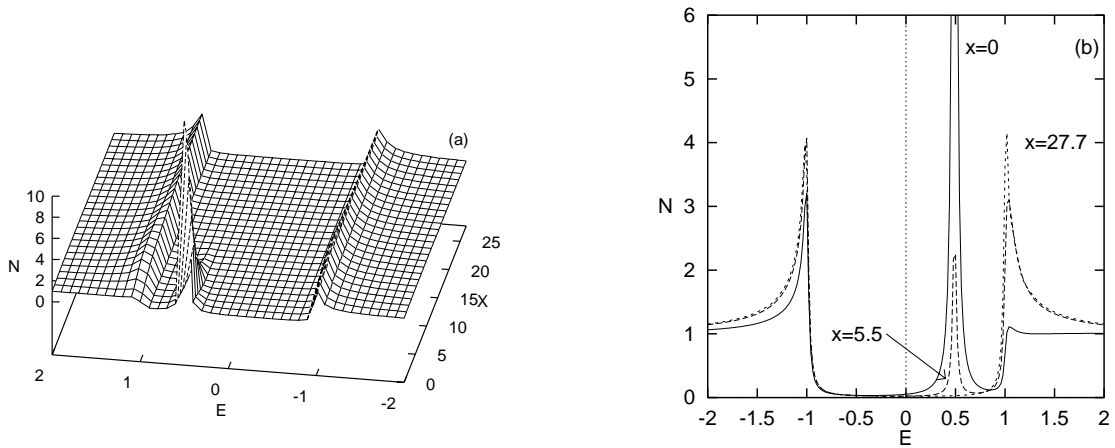


Fig. 3. (a) Local density of states for a fixed momentum, which has been calculated from the self-consistent order parameters. It is normalized by the one in the normal state. The energy  $E$  is scaled by  $\Delta(T)$ . The momentum is chosen to give  $\theta_k = \pi/8$ . A small imaginary part of  $0.02 \times \Delta(T)$  is added to  $E$  for the plotting. (b) Local density of states at various positions.

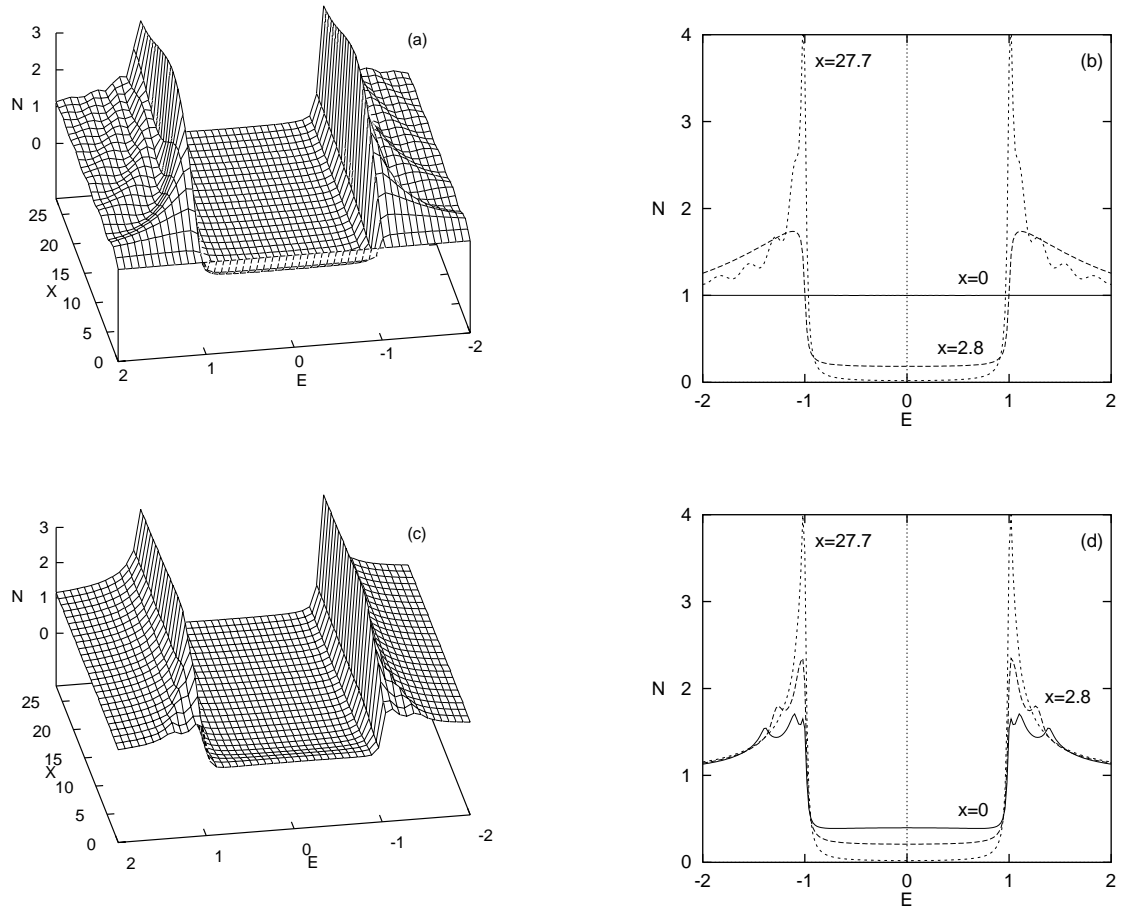


Fig. 4. (a) Total local density of states for uniform order parameters. The vector potential is neglected for simplicity. (b) Total local density of states at various positions of (a). (c) Total local density of states for the self-consistent order parameters, in which the vector potential is taken into account. (d) Total local density of states at various positions of (c).

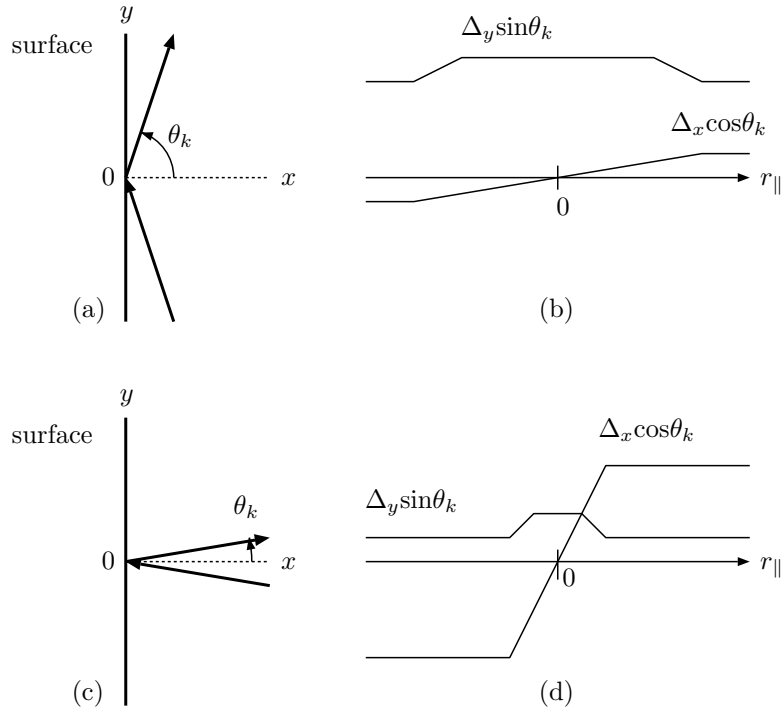


Fig. 5. (a) A classical trajectory of an quasiparticle reflected by a surface. (b) A schematic spatial dependence of the self-consistent order parameters along the classical trajectory.  $r_{\parallel}$  is taken along the classical trajectory. (c) Same as (a) for a smaller  $\theta_k$ . (d) Same as (b) for a smaller  $\theta_k$ .

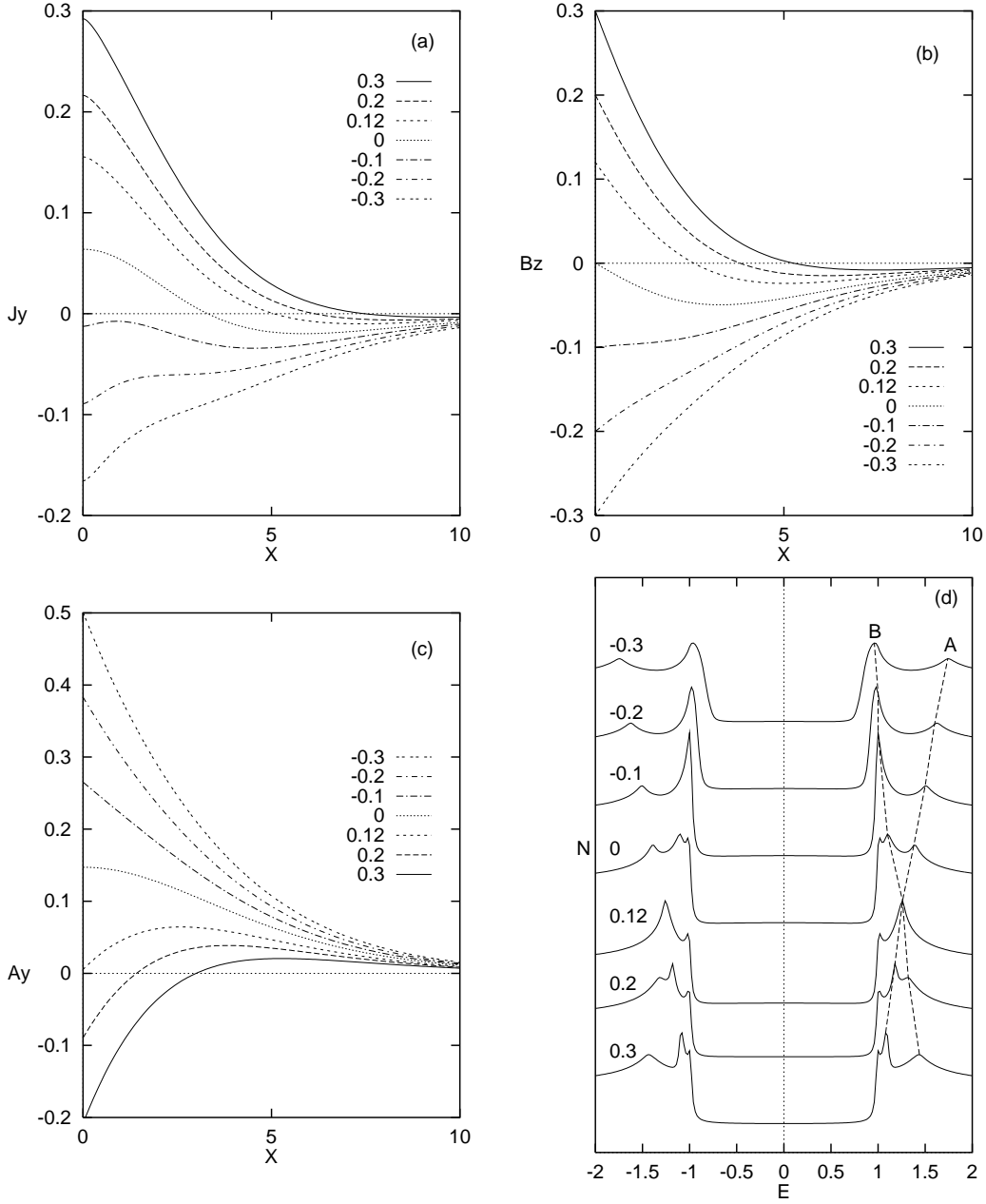


Fig. 6. (a) Spatial dependence of the self-consistent current  $J_y(x)$  which flows along the surface.  $J_y(x)$  and  $x$  are scaled by  $J_0=ev_F N(0)T_C$  and  $\xi_0$ , respectively. The parameters are chosen as  $T=0.2T_C$ ,  $\omega_C=10T_C$ ,  $\kappa=2.5$ . (b) Spatial dependence of the self-consistent magnetic field  $B_z(x)$ , which is scaled by the critical field  $B_C=\Phi_0/2\sqrt{2}\pi\xi_0\lambda_L$ . (c) Spatial dependence of the self-consistent vector potential  $A_y(x)$ , which is scaled by  $\Delta(0)/ev_F$ . (d) Local density of states at  $x=0$  in an arbitrary unit. In each figure the applied external magnetic fields normalized by  $B_C$  are depicted. In the preset case  $B_{c1}/B_C=\log\kappa/\sqrt{2}\kappa\simeq 0.26$ .

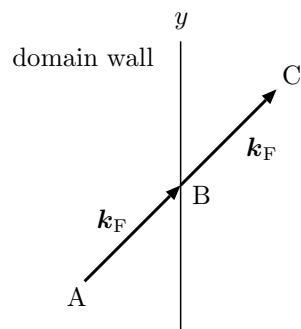


Fig. 7. Classical trajectory of a quasiparticle going through a domain wall, in which the incident momentum is conserved.



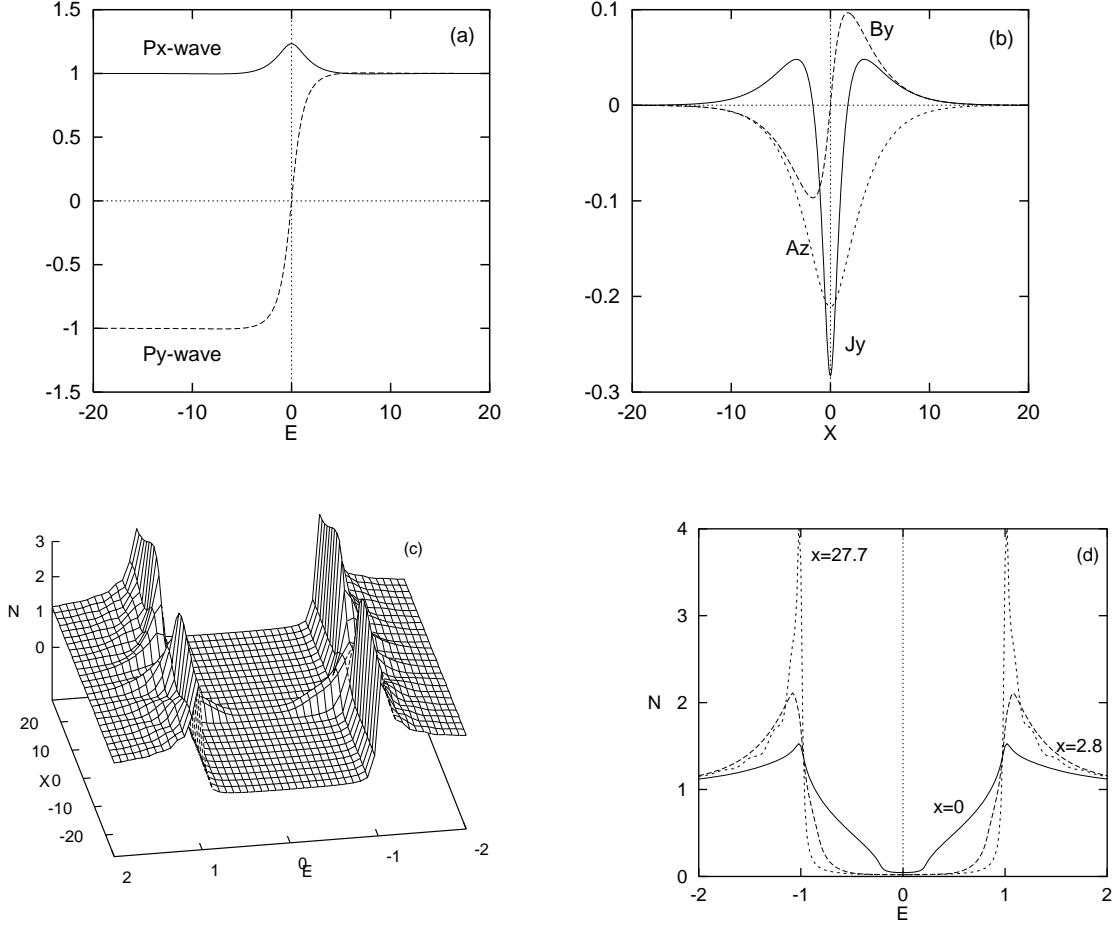


Fig. 8. (a) Spatial dependence of the self-consistent order parameters for  $p_x$ - and  $p_y$ -waves.  $\Delta_x$  and  $\Delta_y$  are real and imaginary, respectively. The set of parameters are chosen as  $T=0.2T_C$ ,  $\omega_C=10T_C$ ,  $\kappa=2.5$ . (b) The self-consistent current density  $J_y(x)$ , the magnetic field  $B_z(x)$  and the vector potential  $A_y(x)$ . They are scaled by  $J_0=ev_F N(0)T_C$ ,  $B_C=\Phi_0/2\sqrt{2}\pi\xi_0\lambda_L$  and  $\Delta(0)/ev_F$ , respectively. (c) Total local density of states. (d) Total local density of states at various positions. They are symmetric under  $x\rightarrow-x$ .

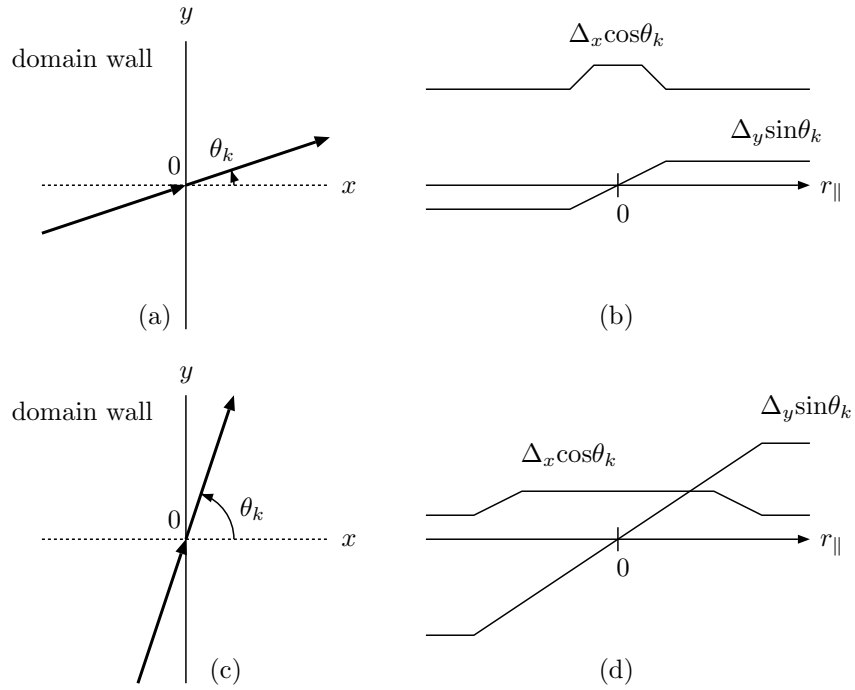


Fig. 9. (a) A classical trajectory of an quasiparticle going through a domain wall. (b) A schematic spatial dependence of the self-consistent order parameters along the classical trajectory.  $r_{||}$  is taken along the classical trajectory. (c) Same as (a) for a larger  $\theta_k$ . (d) Same as (b) for a larger  $\theta_k$ .